Intravital Imaging Study on Photodamage Produced by Femtosecond Near-infrared Laser Pulses *In Vivo*

Sergey N. Arkhipov*[1,2], Ilyas Saytashev[3] and Marcos Dantus[3]

[1]Institute of Fundamental Medicine and Biology, Kazan (Volga Region) Federal University, Kazan, Russia
[2]ITMO University, Saint-Petersburg, Russia
[3]Department of Chemistry, Michigan State University, East Lansing, MI

ABSTRACT

Ultrashort femtosecond pulsed lasers may provide indispensable benefits for medical bioimaging and diagnosis, particularly for noninvasive biopsy. However, the ability of femtosecond laser irradiation to produce biodamage in the living body is still a concern. To solve this biosafety issue, results of theoretical estimations as well as the *in vitro* and *in situ* experiments on femtosecond biodamage should be verified by experimental studies conducted *in vivo*. Here, we analyzed photodamage produced by femtosecond (19, 42 and 100 fs) near-infrared (NIR; ~800 nm) laser pulses with an average power of 5 and 15 mW in living undissected Drosophila larvae (*in vivo*). These experimental data on photodamage *in vivo* agree with the results of theoretical modeling of other groups. Femtosecond NIR laser pulses may affect the concentration of fluorescent biomolecules localized in mitochondria of the cells of living undissected Drosophila larva. Our findings confirm that the results of the mathematical models of femtosecond laser ionization process in living tissues may have a practical value for development of noninvasive biopsy based on the use of femtosecond pulses.

INTRODUCTION

Two-photon excitation (TPE) fluorescence microscopy of scattering tissue has advantages over single-photon fluorescence microscopy: (1) Intrinsic three-dimensional resolution in laser scanning fluorescence microscopy; (2) Fluorescence emission increases quadratically with excitation intensity; (3) Unprecedented capabilities for three-dimensional, spatially resolved photochemistry, *etc.* (1).

However, the fluorescence signal and observation time are limited by phototoxic effects (2,3). The photodamage study on Chinese hamster ovarian cells irradiated with femtosecond laser pulses of the range 120–1000 fs with 10 mW mean power (for 150 fs pulses at 780 nm: 800 W peak power and 1.2×10^{12} W cm^{-2} peak intensity) showed that photodamage strongly depends on pulse duration, following approximately a $P^2 \tau^{-1}$ dependence (where P is mean power and τ is the pulse duration full width at half maximum), and is likely based on a TPE process rather than a one- or a three-photon event (4). Relying on the imaging experiments on rat neocortical neurons stained with

Ca^{2+} indicator dye, another group formulated a power law with an exponent of 2.5 for the rate of fluorescence increase and proposed that a TPE mechanism is mainly responsible for the cumulative photodamage of pulses with duration ≥75 fs. Two similar results were obtained in experiments on bovine adrenal chromaffin cells, stained with Ca^{2+} indicator dye and irradiated with 190 fs pulses at 840 nm. It has been shown that the photodamage threshold is proportional to the integral (over space and time) of laser intensity raised to a power ~2.5 (5). The authors proposed that destructive photodamage of biological samples is caused by a multiphoton process, maybe a mixture of two- and three-photon absorption, or by a two-photon absorption followed by partially saturated secondary process. They suggested that, at low excitation intensities, damage may be dominated by a two-photon absorption process, but higher order mechanisms become important at higher excitation powers, while no significant one-photon absorption (heating) takes place (6).

The opposite conclusion was made in the *in vivo* study, where 120 fs pulses (76 MHz repetition rate) and continuous-wave irradiation were delivered to rhesus's paramacular retinal regions over 0.25 s at 800 nm. Nearly identical damage thresholds indicated a primarily thermal tissue damage mechanism (7). Thermal mechanical damage (the formation of cavitation) associated with one-photon absorption of infrared excitation light by melanin granules was reported in studies on skin specimens (8). The experimentally established thermal mechanical damage threshold was consistent with a simple heat diffusion model for skin under femtosecond pulse laser illumination. In the study from our group, the quantitative analysis of experimental data showed that photodamage, scored as lethality in populations of living Drosophila larvae evaluated 14 days postexposure, following irradiation with 37 or 100 fs laser pulses (1 kHz repetition rate) at 800 nm for 10 min, has a mostly linear character on energy fluence per pulse (9).

Another possible mechanism for the photodamage produced by femtosecond laser pulses is destructive intracellular optical breakdown or ablation (6,10,11). Because ultrashort laser pulses are extensively employed in applications of micro- and nanostructuring, nanosurgery and biophotonics (12,13), there are many experimental studies on various ablation effects, produced by femtosecond laser pulses in living cell and tissues (11,13–20).

Femtosecond pulses may produce ionization of transparent material *via* two different processes: (1) multiphoton ionization and (2) avalanche ionization (17,19,20). Some authors consider these processes to be achieved by the high peak intensity of

these pulses which can reach $\sim 10^{13}$ W cm^{-2} (17). Voronin and Zheltikov estimated the critical number of free electrons generated within the laser–tissue interaction region per photon emitted as nonlinear optical signal (a measure of the "noninvasiveness" of nonlinear optical imaging techniques) for a broad variety of biomarker dyes and bioactivity reporter proteins—the threshold is exceeded above 10^{12} W cm^{-2} (21). For example, ionization of water in the focal volume of a 0.65 NA objective requires 0.1 μJ using 100 fs pulses at 800 nm (15). The use of the high-NA objectives allows production of the ionization and associative ablation using femtosecond pulses with even lower pulse energy or average (mean) power. For example, low millisecond exposure of sub-20 fs 75 MHz near-infrared (NIR) laser pulses with an average power of less than 7 mW (<93 pJ) using an objective with 1.3 NA produced transient nanopores in the cell membranes of human pancreatic and salivary gland stem cells (18). Tight focusing using high numerical aperture microscope objectives allows for reduction in the pulse energy, enhanced precision, and limits additional undesirable nonlinear side effects observed during optical breakdown and plasma formation (self-focusing, filamentation and plasma defocusing) (12).

The energy from the recombination of ions and electrons (separated by ionization) contributes to highly unstable conditions and can lead to a microexplosion, shockwave and bubble formation (15), which result in mechanical disruption of tissues (22,23). Moreover, ionization can also induce chemical reactions, for example the formation of reactive oxygen species and the direct breaking of chemical bonds in cellular structures (17), which can also lead to biological effects in treated cells and tissues (24). For example, NIR 170 fs laser pulses operating at 80 MHz repetition rate and at mean power of >7 mW evoked generation of reactive oxygen species such as H_2O_2 in kidney epithelium cells, leading to their apoptosis-like death (14).

Despite a respectively high number of publications on femtosecond laser photodamage, we found few studies conducted in whole (undissected), unlabeled living animals (*in vivo*). Many *in vitro* studies showing a variety of photodamage processes are set in at similar power levels with similar exponents in suspensions of fluorescently stained living cells (2,5,6,25).

In the present intravital imaging study, we analyzed the photodamage produced by 19, 42 and 100 fs laser pulses at average powers of ~ 5 and ~ 15 mW centered at 800 nm wavelength in the undissected and unlabeled samples of living Drosophila larvae (*in vivo*). Using these experimental conditions, we tested whether the laser–tissue interaction process resulting in photodamage in whole living organism is linear or nonlinear. We also compared our data on the ablation *in vivo* with the predictions of theoretical models of laser ionization.

MATERIALS AND METHODS

Drosophila culture and sample preparation. A wild type strain of *Drosophila melanogaster* (a gift from Dr. Chuck Elzinga of Michigan State University) was used in this study. The flies were grown at room temperature in culture vials with instant Drosophila fly culture media supplemented with yeast (all were purchased from Carolina Biological Supply Company, Burlington, NC). Experiments were performed during the third instar larvae, collected from the upper part of the medium in the vial and rinsed with distilled water and anesthetized with FlyNap (Carolina Biological Supply Company) for 30 min prior to preparation of whole-body (nondissected) samples. For sample preparation we employed our own technique described below. The whole-body samples of living Drosophila larva were prepared by using the protocol developed by us.

An anesthetized larva is placed on the glass slide (VWR International, Radnor, PA), embedded with O.C.T. Compound Tissue-Tek (Sakura Finetek USA Inc., Torrance, CA) and mounted with cover glass No. 1 (Corning Inc., Corning, NY). The larva immobilized inside the mounted preparations is surrounded by spaces occupied with some amount of atmospheric air; this allowed the animal to breath inside the sample during experiment. The mounted sample was allowed to solidify for more than 1 h prior to the procedure of irradiation and imaging. We conducted several preliminary experiments that showed that larvae immobilized in the mounted samples were alive for many hours after solidifying: all the larvae in the disassembled chambers demonstrated active movement and were reactive on mechanical stimuli. Checking the larval heart beat after irradiation with the use of light microscopy also showed aliveness of all the larvae. We used the same methods to verify aliveness of the larvae during the experimental series.

Irradiation of living Drosophila larvae. The ability of ultrashort femtosecond NIR laser pulses with various durations (19, 42 and 100 fs) and intensities to induce photodamage in living tissues of a whole (undissected) organism was tested by placing the whole-body embedded samples of Drosophila larvae under the focused laser pulses (spot diameter ~ 364 nm estimated from diffraction limit) scanned on the pieces of larval inner tissues (32 μm × 32 μm in size, the formal resolution ~ 0.063 μm pixel^{-1}, the scanning amplitude 0.25) for 300 s. Before and after applying this intensive irradiation in the fields of 32 μm × 32 μm in size, the 16-times expanded (128 μm × 128 μm in size, the formal horizontal resolution ~ 0.25 μm pixel^{-1}, the scanning amplitude 1.0) same-centered area of the same sample was additionally scanned for 100 s using the same pulses. Laser irradiation was simultaneously accompanied by imaging of the same fields of larval tissue (see live Drosophila larvae imaging section below).

About half of the irradiated and analyzed tissue samples in each experimental group belonged to larval adipose tissue; other samples were imaginal disks, trachea, salivary gland and mixed tissues. Up to 10 larvae were used to irradiate the tissue samples for each individual group. Experiments were carried out on several groups of the analogous tissue samples according to laser exposure conditions; pulse durations (19, 42 and 100 fs), average power (after the objective) 5 and 15 mW where the peak intensity varies in the range from 1.13×10^{12} to 17.83×10^{12} W cm^{-2} (please see next subsection and Table 1). In order to obtain transform-limited (TL) pulses (19 or 42 fs) in the focus of a high-NA objective, laser pulses were compressed by the multi-iterative measurement and compensation algorithm of the multiphoton intrapulse interference phase scan (MIIPS) software using both quadratic and sinusoidal reference functions; second-order dispersion was superimposed to a TL correction mask for the linearly chirped pulses (42 or 100 fs). According to Comin *et al.* (26), no difference in compensation between MIIPS and its improved version (G-MIIPS) is observed after using a few iterations (please refer to fig. 7 in their paper).

Calculation of peak intensity of femtosecond NIR laser pulses used for irradiation. The intensity of a laser pulse is power divided by the irradiation area. Therefore, for a fixed area, power and intensity have the same Gaussian-shaped profile in the time domain, which can be described by the following expression:

$$P(t) = P_0 \exp(-t^2/t_0^2)$$

where P_0 is a peak power and t_0 is a parameter of a Gaussian function. Conventionally, pulse duration τ is described by a full width at half maximum; it is related to a parameter t_0 as following:

Table 1. Values of the peak intensity calculated for different conditions of pulsed irradiation.

Average power P_{av} (mW)	Peak intensity I_{peak} (TW cm^{-2})		
	19 fs	42 fs	100 fs
5	5.94	2.69	1.13
15	17.83	8.06	3.39

$$\tau = 2\sqrt{(\ln 2)}t_0$$

By integrating the power over the period of a laser pulse, we obtained the expression for pulse energy:

$$E = P_0 t_0 \sqrt{\pi} = 1.064 P_0 \tau$$

On the other hand, the energy on the time period T of a single pulse can be derived as:

$$E = P_{av} \times T = P_{av}/f$$

where average power P_{av} and repetition rate f were measured by a power meter and oscilloscope respectively.

These relationships between pulse energy, repetition rate, pulse duration and average power provide us with the calculation of a peak power:

$$P_0 = P_{av}/(1.064 f \tau)$$

The intensity profile in the spatial domain can be described as follows:

$$I(x, y) = I_{peak} \exp(-8(x^2 + y^2)/d^2)$$

where I_{peak} is the peak intensity and d is a beam waist.

By integrating the intensity over the pulse area, we obtain the relationship between peak intensity and peak power. Because the laser beam was tightly focused into a spot that has a size of light diffraction limit, we calculated a value of the beam waist using Abbe's formula:

$$d = \lambda/2NA$$

where λ is the wavelength of the light and NA is numerical aperture of the objective lens. For our conditions ($\lambda = 800$ nm, NA = 1.1), the beam waist $d = 364$ nm.

$$I_{peak} = 8P_0/(\pi d^2)$$

$$I_{peak} = 8P_{av}/(1.064 f \tau \pi d^2)$$

Values of the peak intensity calculated for different conditions of pulsed irradiation are presented in Table 1.

Imaging of living Drosophila larvae. Two-photon imaging of whole-body samples of nonlabeled larval tissues was carried out simultaneously with irradiation. Two-photon fluorescence images of the tissues of embedded living larvae were acquired using an inverted Eclipse TE-2000 (Nikon, Japan) microscope equipped for multiphoton imaging with a water-immersion LD C-Apochromat 40 × /1.1 W Corr Objective (Carl Zeiss, Germany), 80 MHz repetition rate broadband Ti: Sapphire Laser (Kapteyn-Murnane Laboratories, Inc., Boulder, CO) with pulses centered at 800 nm, pulse shaper with MIIPS adaptive pulse compression, galvanometric scanner QuantumDrive-1500 (Nutfield Technology, Inc.), dichroic mirror, shortpass emission filter (both from Chroma Technology Corp.) and photomultiplier tube detector HC120-05MOD (Hamamatsu, Japan). The average power of the excitation beam was measured with a FieldMaxII-TOP power meter (Coherent, Santa Clara, CA) after the objective; prior to imaging, pulses were compressed to be close to TL and pulse duration was measured ∼ 19 fs after the objective using the pulse shaper. LabVIEW 7.1 software (National Instruments) developed in our laboratory was used to acquire images, 128 μm × 128 μm in size (the formal horizontal resolution ∼0.25 μm pixel^{-1}, the scanning amplitude 1.0) and 32 μm × 32 μm (the formal horizontal resolution ∼0.063 μm pixel^{-1}, the scanning amplitude 0.25). The imaging was conducted simultaneously (in the same procedure) with femtosecond laser irradiation (please see the subsection on the irradiation of living Drosophila larvae).

Image processing and analysis. In general, one hundred 1-s frames for each one-section view were averaged and transformed into 8-bit format to generate each final image using the program ImageJ (National Institute of Mental Health, Bethesda, MD). Adobe Photoshop 12.04 (Adobe Systems Inc.) was then used for further adjustments of the brightness in the final images. Thus, for each imaged/irradiated area of tissue, we produced five final images: two (original and final) and three intermediate images, obtained respectively at the scanning amplitude 1.0 (the scanning field 128 μm × 128 μm, the formal resolution ∼0.25 μm pixel^{-1}) and 0.25 (the scanning field 32 μm × 32 μm, the formal resolution ∼0.063 μm pixel^{-1}). Amplitude 0.25 provides 16 times more pulses per diffraction-limited irradiation spot. The fluorescence images with satisfactory fluorescent signal and contrast were used for scoring and analysis of photodamage.

RESULTS

Effects of irradiation of live larvae with 19 fs NIR laser pulses with average power 15 mW

Intensive irradiation using TL NIR pulses with duration 19 fs and peak power 9.3 kW at scanning amplitude 0.25 induced photodamage in all samples of irradiated living tissues (100%, $N = 16$). The damage was observed as bubble formation, resulting in the ruptures of cellular plasma membranes ("merging cells"), and in following partial or complete ablation of the tissue in the irradiated area (Fig. 1B–E).

The photodamage was consequently accompanied by two kinds of enhancement of endogenous fluorescence. The first, earlier intracellular photoenhancement with characteristic "mitochondria-co-localized" pattern was observed on the periphery of the cell's cytoplasm until the plasma membrane was destroyed by irradiation. Intracellular photoenhancement is replaced by the enhancement of fluorescence in the destroyed tissues (postdamage photoenhancement). Signs of cellular damage appeared in the living tissue within a few seconds after starting laser irradiation (median: 6 s, mean ± SD: 8 ± 8 s).

The zone of photodamage and postdamage photoenhancement was found to spread out into the surrounding nondestroyed tissues, suggesting that this fluorescence could emanate from postdamage cell lysates. Only one adipose tissue sample showed photodamage of cellular membranes without significant photoenhancement. Only two samples had the homogeneous (without characteristic pattern) photoenhancement in cytoplasm of the cells with undamaged plasma membranes. We consider this intracellular homogeneous photoenhancement in the cells with undamaged plasma membranes to be a sign of destruction of the intracellular membranes (of organelles and compartments). The use of the same pulses at the scanning amplitude 1.0 (the dwell time is 16 times lower than at scanning amplitude 0.25) dramatically reduced photodamage in irradiated living tissues (Fig. 1A).

Effects of irradiation of live larvae with 42 fs NIR laser pulses with average power 15 mW

The longer (42 fs) TL and chirped (chirp: ∼258 fs^2) NIR pulses of the same average power (peak power ∼4.2 kW) and scanning amplitude 0.25 also produced bubble formation, accompanied by subcellular and postdamage photoenhancement in all samples (100%, $n = 21$); however, the area and intensity of photodamage were smaller and did not spread beyond the area of irradiation as in the previous experiments (Fig. 1G–K, M–P).
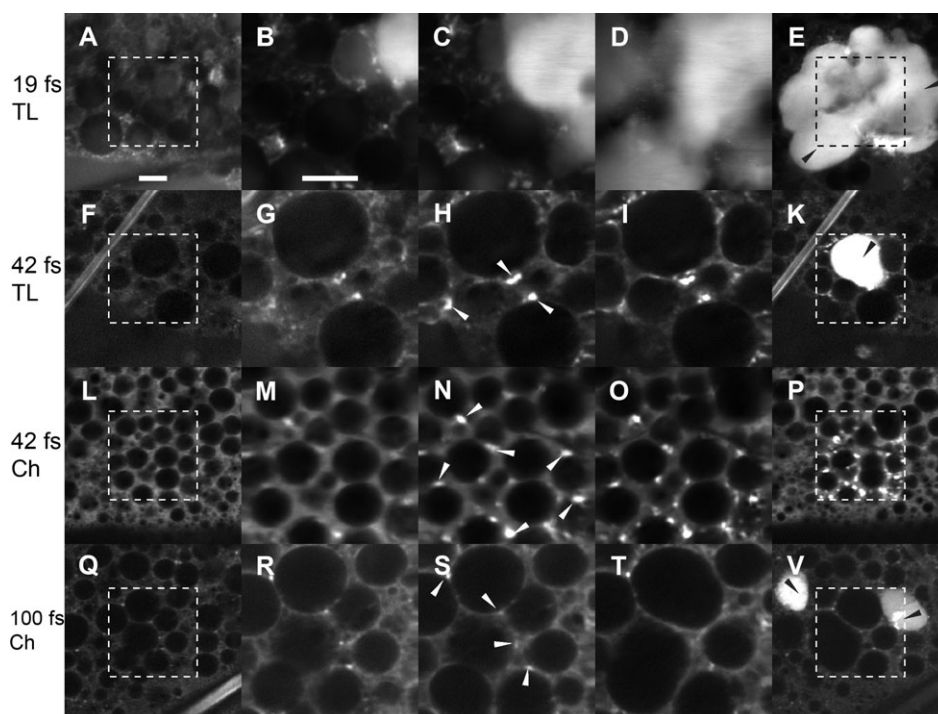
Figure 1. Fluorescence images of tissues of living nondissected Drosophila larvae, obtained with the use of femtosecond NIR pulses of different pulse duration and same average power (15 mW). The panels represent the images of four samples. Each image is produced by summation of one hundred 1-s frames of the same optical section of the sample. Each row represents a sequence of images, obtained with use of pulses of different durations. First and last columns consist of images received in the beginning (panels A, F, L and Q) and the end (E, K, P and V) of imaging experiments at scanning amplitude 1.0. The middle three columns (panels B–D, G–I, M–O and R–T) represent a sequence of three images (for each sample) received at amplitude 0.25 which provides 16 times more pulses per time in the smaller area of irradiation scanned for 300 s, centered as the images obtained at amplitude 1.0 (indicated by white dotted squares in the panels of the first and last columns). Each image of columns is produced by summation of one hundred 1-s frames of the same optical section of the sample. Photoenhancement, accompanied by photodamage in the irradiated tissues (indicated by black arrowheads in panels E, K and V), usually spreads over the central area (scanned at amplitude 0.25). Intracellular photoenhancement without visible damage of cellular membranes (indicated by white arrowheads in panels C, G, N and S) resembles the localization pattern of mitochondria in the cells. Scale bar: 10 μm.

Irradiation with 42 fs pulses required significantly longer time (median: 99 s, mean ± SD: 107 ± 65 s) to induce bubble formation in the samples than the analogous treatment with 19 fs pulses ($P < 0.001$, two-tailed U-test). The subgroups of samples treated with the TL (median: 99 s, mean ± SD: 102 ± 70 s) and chirped pulses (median: 104 s, mean ± SD: 115 ± 59 s) did not differ by this parameter ($P > 0.05$, two-tailed U-test).

In scoring photodamage in the samples ($N = 32$) by criterion of ruptured plasma membranes ("merging cells"), we found that 75% were affected. The levels of photodamage in subgroups of the samples treated with the TL ($N = 13$) (Fig. 1G–K) and chirped pulses ($N = 19$) (Fig. 1M–P) were comparable: 77% and 74%, respectively.

During irradiation of the remaining samples, the cells acquired intracellular photoenhancement with characteristic patterns on the periphery of the cytoplasm. When the samples were irradiated with the same pulses at scanning amplitude 1.0 (the dwell time is 16 times lower than at scanning amplitude 0.25), we observed stable high-contrast fluorescent images without visible mechanical photodamage (Fig. 1F,L).

Effects of irradiation of live larvae with 100 fs NIR laser pulses with average power 15 mW

Irradiation with 100 fs chirped (chirp: ~669 fs^2) NIR laser pulses with average power 15 mW (peak power ~1.8 kW) at the

scanning amplitude 0.25 demonstrated an even lower frequency of photodamage in the living samples: four of seven (~57%) of the samples available for analysis of the bubble formation experienced bubbling, while six of 17 (~35%) of the samples were found to be positive by the criterion of ruptured plasma membranes (Fig. 1R–V).

The time for the manifestation of photodamage in the living tissue (median: 226 s, mean ± SD: 224 ± 36 s) was significantly longer ($P < 0.01$, two-tailed U-test) than for 42 fs pulsed irradiation and dramatically extended ($P < 0.001$, two-tailed U-test), compared to 19 fs pulses. Intracellular and postdamage photoenhancements were found to be much less intensive and less stable than in the analogous samples irradiated with 42 fs pulses. In some samples, the limited postdamage photoenhancement was found migrating through extracellular space of the cells with nondamaged plasma membranes. The samples irradiated with these pulses at scanning amplitude 1.0 (the dwell time is 16 times lower than at the scanning amplitude 0.25) provided stable contrast images without visible photodamage (Fig. 1Q).

Effects of irradiation of live larvae with femtosecond NIR laser pulses with average power 5 mW

Two-photon imaging of larval tissues with ~5 mW femtosecond NIR laser pulses with durations 19 and 42 fs (peak power ~3.1 and ~1.4 kW, respectively) for 100–300 s produced stable and

high-contrast fluorescence images without visible photodamage on the level of cellular pattern (Fig. 2).

The images produced with the shorter pulses were generally brighter and of higher contrast. A weak intracellular photoenhancement could be found in the samples. Imaging with 100 fs NIR laser pulses of the same average power 5 mW (peak power ~0.6 kW) did not provide images with satisfactory signal and contrast under our experimental conditions (data not shown).

DISCUSSION

To interpret our experimental results, obtained from whole undissected unlabeled animals (*in vivo*), we employed the equation which describes the dependence of the photodamage on energy and pulse duration in living cells *in vitro* (4), and was used by us previously for scoring lethality, rates of necrosis and apoptosis in population of living Drosophila larvae exposed to femtosecond laser pulses (9):

$$S(n) = E^n / \tau^{n-1}$$

where S is the normalized nonlinear effect of irradiation, n is average order of the photonic process involved in photodamage, E is the energy fluence per pulse (J m^{-2}) and τ is the pulse duration. According to this equation, in case of linear process ($n = 1$), the pulses of different peak powers and pulse duration but the same average power should provide the same levels of photodamage. Observation of qualitatively and quantitatively different effects of irradiation with femtosecond NIR laser pulses of different durations but the same average power 15 mW (Fig. 1) provides evidence that laser–tissue interaction within the scored range of peak powers is a nonlinear process.

Because pulsed irradiation at 5 mW did not produce any visible ablation, bubble formation or tissue disruption in our experiments (Fig. 2), we are not able to make the same conclusion for these pulses relying only on mechanical photodamage. However, this suggestion could be correct, considering photoenhancement as an indication of femtosecond photodamage (27,28), and observing different degrees of photoenhancement (Fig. 2) produced by femtosecond pulses of different durations at the same average power (5 mW).

Tissue ablation is generally considered to be a result of multiphoton ionization and associated plasma formation (6,10,11,17,19,20). In this study, calculation of peak powers of femtosecond laser pulses showed tissue ablation in whole undissected unlabeled living organisms at the range of peak intensities (~10^{12}–10^{13} W cm^{-2}) predicted by the theoretical models (15,17,21). This confirms that femtosecond pulses may produce multiphoton ionization (~10^{12} W cm^{-2}) and avalanche ionization (~10^{13} W cm^{-2}) *in vivo*, and supports our conclusion that the femtosecond laser-induced photodamage *in vivo* is a nonlinear process.

The rise of fluorescence (photoenhancement) experimentally observed by us and by others (27–29) reflects the reducing of nonfluorescent NAD+ into fluorescent NADH (25,28,30,31). A pattern of so-called "punctuated fluorescence," observed by us in our intravital experiments and by others (13,32,33), confirms that fluorescent organelles irradiated with femtosecond pulses *in vivo* are likely mitochondria (33), and should be also considered in the course of developing safer intravital noninvasive imaging.
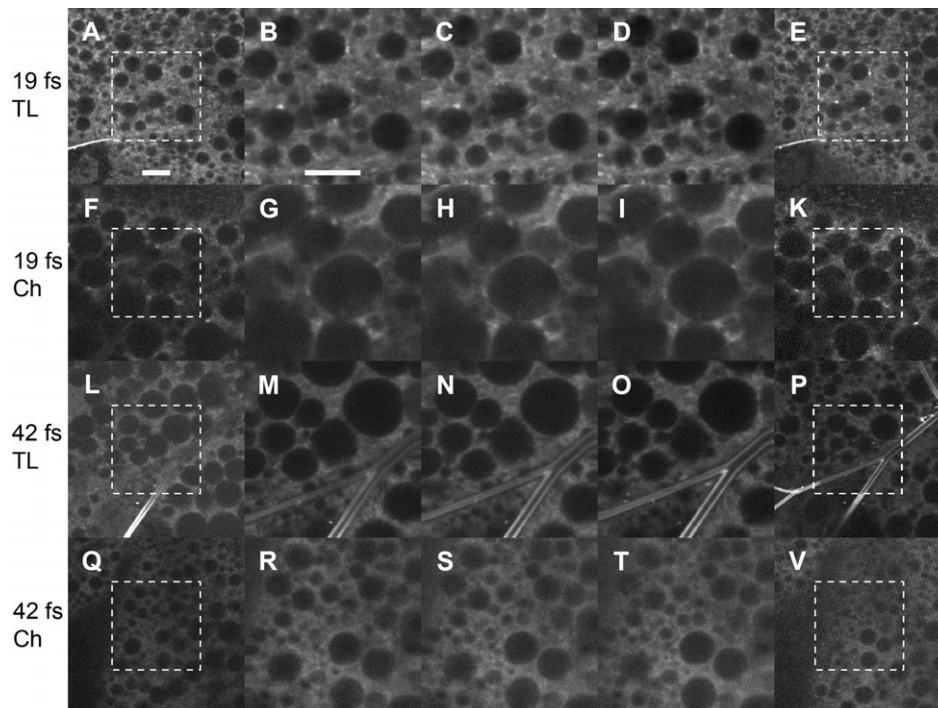
Figure 2. Fluorescence images of tissues of living nondissected Drosophila larvae, obtained with the use of 5 mW femtosecond pulses with 19 and 42 fs pulse duration (peak power ~3.0 and ~1.4 kW, respectively). Basic conventions are essentially the same as in the previous figure. Scale bar: 10 μm.

REFERENCES

1. Denk, W., J. H. Strickler and W. W. Webb (1990) Two-photon laser scanning fluorescence microscopy. *Science* **248**, 73–76.
2. Koester, H. J., D. Baur, R. Uhl and S. W. Hell (1999) Ca2 + fluorescence imaging with pico- and femtosecond two-photon excitation: signal and photodamage. *Biophys. J.* **77**, 2226–2236.
3. Eggeling, C., A. Volkmer and C. A. Seidel (2005) Molecular photobleaching kinetics of Rhodamine 6G by one- and two-photon induced confocal fluorescence microscopy. *Chemphyschem* **6**, 791–804.
4. König, K., T. W. Becker, P. Fischer, I. Riemann and K. J. Halbhuber (1999) Pulse-length dependence of cellular response to intense near-infrared laser pulses in multiphoton microscopes. *Opt. Lett.* **24**, 113–115.
5. Hopt, A. and E. Neher (2001) Highly nonlinear photodamage in two-photon fluorescence microscopy. *Biophys. J.* **80**, 2029–2036.
6. König, K., U. Simon and K. J. Halbhuber (1996) 3D resolved two-photon fluorescence microscopy of living cells using a modified confocal laser scanning microscope. *Cell. Mol. Biol. (Noisy-le-grand)* **42**, 1181–1194.
7. Thomas, R. J., G. D. Noojin, D. J. Stolarski, R. T. Hall, C. P. Cain, C. A. Toth and B. A. Rockwell (2002) A comparative study of retinal effects from continuous wave and femtosecond mode-locked lasers. *Lasers Surg. Med.* **31**, 9–17.
8. Masters, B. R., P. T. So, C. Buehler, N. Barry, J. D. Sutin, W. W. Mantulin and E. Gratton (2004) Mitigating thermal mechanical damage potential during two-photon dermal imaging. *J. Biomed. Opt.* **9**, 1265–1270.
9. Saytashev, I., S. N. Arkhipov, N. Winkler, K. Zuraski, V. V. Lozovoy and M. Dantus (2012) Pulse duration and energy dependence of photodamage and lethality induced by femtosecond near infrared laser pulses in *Drosophila melanogaster*. *J. Photochem. Photobiol. B* **115**, 42–50.
10. Oraevsky, A. A., L. B. Da Silva, A. M. Rubenchik, M. D. Feit, M. E. Glinsky, M. D. Perry, B. M. Mammini, W. Small and B. C. Stuart (1996) Plasma mediated ablation of biological tissues with nanosecond-to-femtosecond laser pulses: relative role of linear and 20 nonlinear absorption. *IEEE J. Sel. Top. Quantum Electron.* **2**, 801–809.
11. Watanabe, W., N. Arakawa, S. Matsunaga, T. Higashi, K. Fukui, K. Isobe and K. Itoh (2004) Femtosecond laser disruption of subcellular organelles in a living cell. *Opt. Express* **12**, 4203–4213.
12. Arnold, C. L., A. Heisterkamp and H. Lubatschowski (2009) Computational model for nonlinear plasma formation in high NA micromachining of transparent materials and biological cells. *J. Laser Micro Nanoen.* **4**, 39–44.
13. Kuetemeyer, K., R. Rezgui, H. Lubatschowski and A. Heisterkamp (2010) Influence of laser parameters and staining on femtosecond laser-based intracellular nanosurgery. *Biomed. Opt. Express* **1**, 587–597.
14. Tirlapur, U. K. and K. Konig (2001) Femtosecond near-infrared laser pulse induced strand breaks in mammalian cells. *Cell. Mol. Biol. (Noisy-le-grand)*, **47** (Online Pub), OL 131–OL 134.
15. Schaffer, C. B., N. Nishimura, E. N. Glezer, A. M. T. Kim and E. Mazur (2002) Dynamics of femtosecond laser-induced breakdown in water from femtoseconds to microseconds. *Opt. Express* **10**, 196–203.
16. Kohli, V., A. Y. Elezzabi and J. P. Acker (2005) Cell nanosurgery using ultrashort (femtosecond) laser pulses: applications to membrane surgery and cell isolation. *Lasers Surg. Med.* **37**, 227–230.
17. Nishimura, N., C. B. Schaffer and D. Kleinfeld (2006) In vivo manipulation of biological systems with femtosecond laser pulses. *Proc. SPIE* **6261**, 62611J.
18. Uchugonova, A., K. Konig, R. Bueckle, A. Isemann and G. Tempea (2008) Targeted transfection of stem cells with sub-20 femtosecond laser pulses. *Opt. Express* **16**, 9357–9364.
19. Kalies, S., K. Kuetemeyer and A. Heisterkamp (2011) Mechanisms of high-order photobleaching and its relationship to intracellular ablation. *Biomed. Opt. Express* **2**, 805–816.
20. Jiao, J. and Z. Guo (2012) Analysis of plasma-mediated ablation in aqueous tissue. *Appl. Surf. Sci.* **258**, 6266–6271.
21. Voronin, A. A. and A. M. Zheltikov (2010) Ionization penalty in nonlinear optical bioimaging. *Phys. Rev. E* **81**, 051918.
22. Venugopalan, V., A. 3rd Guerra, K. Nahen and A. Vogel (2002) Role of laser-induced plasma formation in pulsed cellular microsurgery and micromanipulation. *Phys. Rev. Lett.* **88**, 078103.
23. Vogel, A. and V. Venugopalan (2003) Mechanisms of pulsed laser ablation of biological tissues. *Chem. Rev.* **103**, 577–644.
24. Vogel, A., J. Noack, G. Huttman and G. Paltauf (2005) Mechanisms of femtosecond laser nanosurgery of cells and tissues. *Appl. Phys. B* **81**, 1015–1047.
25. König, K., H. Liang, M. W. Berns and B. J. Tromberg (1995) Cell damage by near-IR microbeams. *Nature* **377**, 20–21.
26. Comin, A., R. Ciesielski, G. Piredda, K. Donkers and A. Hartschuh (2014) Compression of ultrashort laser pulses via gated multiphoton intrapulse interference phase scans. *JOSA B* **31**, 1118–1125.
27. Galli, R., O. Uckermann, E. F. Andresen, K. D. Geiger, E. Koch, G. Schackert, G. Steiner and M. Kirsch (2014) Intrinsic indicator of photodamage during label-free multiphoton microscopy of cells and tissues. *PLoS One* **9**, e110295.
28. Pestov, D., Y. Andegeko, V. V. Lozovoy and M. Dantus (2010) Photobleaching and photoenhancement of endogenous fluorescence observed in two-photon microscopy with broadband laser sources. *J. Opt.* **12**, 084006.
29. Débarre, D., N. Olivier, W. Supatto and E. Beaurepaire (2014) Mitigating phototoxicity during multiphoton microscopy of live Drosophila embryos in the 1.0–1.2 μm wavelength range. *PLoS One* **9**, e104250.
30. Eng, J., R. M. Lynch and R. S. Balaban (1989) Nicotinamide adenine dinucleotide fluorescence spectroscopy and imaging of isolated cardiac myocytes. *Biophys. J.* **55**, 621–630.
31. Chance, B., P. Cohen, F. Jobsis and B. Schoener (1962) Intracellular oxidation-reduction states in vivo. *Science* **137**, 499–508.
32. König, K., P. T. So, W. W. Mantulin, B. J. Tromberg and E. Gratton (1996) Two-photon excited lifetime imaging of autofluorescence in cells during UVA and NIR photostress. *J. Microsc.* **183**, 197–204.
33. Masters, B. R., P. T. So and E. Gratton (1997) Multiphoton excitation fluorescence microscopy and spectroscopy of in vivo human skin. *Biophys. J.* **72**, 2405–2412.